Clays and Clay Minerals, Vol. 40, No. 6, 629–643, 1992.

DECOMPOSITION OF X-RAY DIFFRACTION PATTERNS: A CONVENIENT WAY TO DESCRIBE COMPLEX I/S DIAGENETIC EVOLUTION

BRUNO LANSON[1] AND BRUCE VELDE

Laboratoire de Géologie, Ecole Normale Supérieure, 24 rue Lhomond, 75231 Paris Cedex 05, France

Abstract—Decomposition of complex X-ray diffraction profiles is used on well characterized (image analysis of transmission electron micrographs, X-ray fluorescence chemical analyses) diagenetic samples from the Paris basin. The simultaneous occurrence of three "illitic" phases (mixed-layer illite/smectite or I/S, poorly crystallized illite, and mica-like phase) is shown on the various diffraction peaks of the 2–50 °2θ CuKα (44–1.8 Å) range. However, because of theoretical and experimental constraints, it is easier to perform the decomposition routine in the 5–11 °2θ CuKα (17.6–8.0 Å) range. The identification (i.e., illite content and mean coherent scattering domain size) of the various phases is performed by comparing the associated elementary peak characteristics (position, full width at half maximum intensity) with simulated X-ray patterns. When available, the characteristics obtained from the various angular regions are mutually consistent; however, the precise structures of smectite and illite end-members, on the one hand, and the structure of I/S crystallites, on the other hand, are not well known. Consequently, on some angular regions, there is a discrepancy between the characteristics obtained on experimental and calculated X-ray profiles. The definition of more realistic simulation hypotheses for I/S minerals, and for other interstratified clay minerals, would make this powerful and reliable tool to describe X-ray patterns a precise and sensitive identification tool even for complex clay parageneses.

Key Words—Decomposition, Diagenesis, Illite, Illite/smectite, Mixed-layering, Simulation, X-ray powder diffraction.

INTRODUCTION

The extensively described smectite-to-illite diagenetic evolution is not as simple a transformation as it is widely assumed when depicted schematically by a simple illite content *vs* depth trend. An important kinetic effect has been shown by comparing, in various sedimentary basins, the evolution of mixed-layer illite/smectite (I/S) with the maximum temperature experienced by the sediments (Lahann, 1980; Srodon and Eberl, 1984; Velde, 1985; Velde *et al.*, 1986; Jennings and Thompson, 1986; Freed and Peacor, 1989), and/or with organic matter maturation (Smart and Clayton, 1985; Velde and Espitalié, 1989; Francu *et al.*, 1989). As a result of this kinetic effect, the late stage diagenetic clay mineral assemblages in the Paris basin contain several phases* (I/S phases) with distinct, but closely related crystallographic characteristics (Lanson and Champion, 1991). Taking into account the coexistence and simultaneous evolution of randomly interstratified and ordered I/S, Velde and Vasseur (1992) proposed a kinetic model for this transformation based on two first-order reactions (random to ordered I/S, and ordered I/S to illite) to obtain a simplified (e.g, the illite growth is not taken into account) but realistic description of such complex systems.

Because of the coexistence of several argillaceous phases in the same sample, X-ray diffraction (XRD) patterns of diagenetic series most often contain partially overlapping peaks representative of mixed-layered I/S, illite, mica, and occasionally chlorite. The separation of the contributions from these different phases is essential for their characterization by most of the usual identification methods (Srodon, 1979; Velde *et al.*, 1986; Watanabe, 1981, 1988; Tomita *et al.*, 1988; Moore and Reynolds, 1989). Other methods of interpretation require measurements on higher-angle peaks (Srodon, 1980, 1981, 1984), and they are difficult to perform routinely because of the low intensity of these peaks and frequent overlap with other phases. The trial and error crystallographic simulation approach, widely used on monophasic samples (Tchoubar, 1980; Besson, 1980; Pons *et al.*, 1981, 1982; Ben Hadj-Amara *et al.*, 1987) as well as on pure mixed-layer minerals (Sakharov and Drits, 1973; Reynolds, 1980; Srodon, 1980 and 1984; Inoue *et al.*, 1990; Drits *et al.*, 1990), may also be used to model complex polyphasic XRD profiles (e.g., Lanson and Besson, 1992). However, this method is so time-consuming that its routine application on dozens of samples is unrealistic.

Lanson (1990, 1992) developed a decomposition

[1] Present address: EAP-CSTJF, Laboratoire de Géochimie Minérale, 64018 Pau Cedex, France.

* In this paper, the word "phase" describes a population of particles whose physicochemical characteristics vary about a mean value. It is assumed that this population behaves as a monophasic material (in a thermodynamic sense) having the same mean characteristics. Consequently this word is used in the thermodynamic sense throughout the paper for this material.

Copyright © 1992, The Clay Minerals Society

https://doi.org/10.1346/CCMN.1992.0400602 Published online by Cambridge University Press

program for X-ray profiles of clay minerals that enables the separation of the contributions of various phases to the diffracted intensity. This decomposition program can fit a peak on the experimental XRD pattern with up to six elementary curves related to the different phases in the sediment. The position and full width at half maximum intensity (FWHM) of these elementary curves are used to identify each phase by comparison with simulated patterns. Very minor experimental limitations (see below) make this decomposition method a powerful and reliable tool to describe X-ray patterns (Lanson and Besson, 1992). However, because of the very specific characteristics presented by clay minerals XRD profiles, commercially available numerical treatment packages are to be used with caution (Lanson, 1992).

In the low-angle region (5–11 °2θ CuKα; 17.6–8.0 Å) the diffraction peaks of monophasic I/S are symmetrical despite the theoretical restrictions (Lanson and Besson, 1992). In the present paper it is shown that the peak symmetry exists also in higher angle region (e.g., 45.3 °2θ CuKα; 2.00 Å). In spite of contrary statements (Howard and Preston, 1989; Stern *et al.*, 1991), the Gaussian shape is also shown to be well adapted to describe poorly crystallized illite and I/S peaks, while mica and chlorite peaks are more Lorentzian (usually modified Lorentzian). Consequently, it is recommended that one uses a decomposition program that incorporates different functions or combinations of them at the same time. The use of a function including a shape parameter (e.g., Pearson7 or Voigt) is not recommended when fitting higher angle regions (15–50 °2θ CuKα; 5.9–1.8 Å).

Lanson and Champion (1991) used the decomposition program developed by Lanson (1990, 1992) on the 5–11 °2θ CuKα (17.6–8.0 Å) range to show the simultaneous occurrence of three "illitic" phases in their Paris basin samples and to follow their evolution with burial. However, major discrepancies between the FWHM of experimental and simulated patterns, described previously by Reynolds and Hower (1970) and Reynolds (1989), do not permit the precise identification of these phases (Lanson, 1990). The present paper does not solve this peak width problem. Instead, it attempts to extend the work of Lanson and Besson (1992) by looking at higher-angle (15–50 °2θ CuKα; 5.9–1.8 Å) peaks of the I/S phases to show: 1) that it is possible to demonstrate the existence of the three illitic phases with the decomposition of any of these peaks; 2) that because of theoretical and experimental constraints, information on the composition of the illitic phases and their crystallinity is easier to obtain on the 5–11 °2θ CuKα (17.6–8.0 Å) range rather than at higher angles; 3) that it is possible to match the FWHM of experimental and simulated patterns and, thus, to identify precisely the various I/S phases when looking at the 26.75 °2θ CuKα (3.33 Å) and the 45.3 °2θ CuKα (2.00 Å) regions; 4) that the characteristics (illite content and mean coherent scattering domain size) of the various I/S phases obtained from the angular regions studied (5-11 °2θ CuKα; 17.6–8.0 Å; 17.7 °2θ CuKα, 5.00 Å; 26.75 °2θ CuKα; 3.33 Å; 45.3 °2θ CuKα; 2.00 Å) are mutually consistent when available; and 5) that, if the agreement between experimental and simulated I/S patterns is good in the higher angle region (25–50 °2θ CuKα; 3.55–1.8 Å), there are major differences not only in the 5–11 °2θ CuKα (17.6–8.0 Å) range but also in the 17.7 °2θ CuKα (5.00 Å) region.

EXPERIMENTAL METHODS

Samples

The samples studied are drill cuttings from the 2150 m deep borehole C in the eastern Paris Basin near the town of Nancy (supplied by the Institut Français du Pétrole). Lanson and Champion (1991) described the stratigraphic sequence. Characteristic XRD patterns of oriented air-dried (AD) samples from this borehole are shown in Figure 1. Four samples, characteristic of the I/S transition stages, were selected from the original sixty two used to define the general diagenetic trend. The essential criterion for their selection (from 1000, 1550, 1730, and 2130 m depths) was the absence, or the very low abundance, of accessory phases such as chlorite, kaolinite or carbonates (Lanson and Champion, 1991).

In order to constrain the number of elementary peaks to be fitted on the various diffraction maxima of the experimental patterns, it was necessary to get additional information based on direct observation methods to determine the actual number of phases present in the sample. Lanson and Champion (1991) performed TEM morphological studies on the samples used for this paper and identified two populations of particles: lath-shaped particles and hexagonal plates. Analyzing individual particles by X-ray fluorescence (Energy Dispersive Spectroscopy) on TEM they established that the chemical compositions of the two particle types are different. The chemical composition of the laths was consistent with an I/S structure and varied as a function of depth, indicating a decrease in their smectite content. The composition of hexagonal plates was that of illite and did not change with depth. Throughout the sequence they showed, using decomposition of XRD profiles, the coexistence of the I/S mixed-layer phase, the illite phase, and a mica-like phase, as well as occasional chlorite and/or kaolinite. The micaceous phase was assumed by these authors to be detrital because it was present near the surface and showed no evolution with depth. This phase was related to a few irregular thick (highly absorbing) grains observed on TEM; however, one should note that it is unrealistic, even with a decomposition program, to distinguish the respective contributions to an XRD

https://doi.org/10.1346/CCMN.1992.0400602 Published online by Cambridge University Press

profile of a detrital muscovite and of a well-crystallized authigenic illite. The "detrital" label given by Lanson and coworkers to this micaceous phase is based only on a "crystallinity" criterion (FWHM of the diffraction peak) and may not be valid. In the present paper, this well-crystallized micaceous phase is called mica-like phase to avoid any assumptions on its origin.

For the present study, eight additional samples (from 300, 350, 1080, 1305, 1475, 1645, 1850, and 1945 m depths) representative of the diagenetic trend were added to the four studied in detail by Lanson and Champion (1991) in order to provide an expanded evaluation of the decomposition method. The morphological and chemical data available on the Lanson and Champion samples (1991) were also important as an independent control on the results deduced from XRD profile numerical treatment, especially so to check the number of independent phases contributing to the diffraction intensity of the peaks.

An additional sample (WS7–115.45 m) was selected from the hydrothermal series of samples studied by Inoue *et al.* (1978, 1987, 1988), Inoue and Utada (1983), and Inoue (1986) to check the experimental peak shape. This sample is an 85% illite I/S (R = 3).

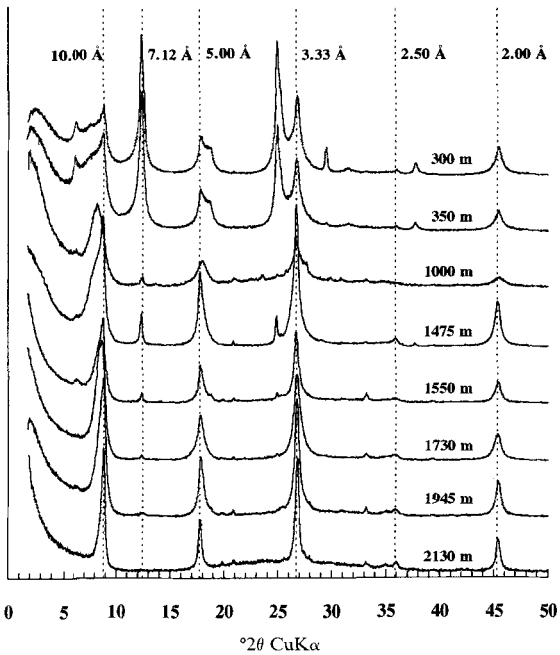


Figure 1. Examples of XRD patterns of oriented, air-dried clay samples from the deep well in the Paris Basin, France.

Sample preparation and processing

The <2 μm fraction was separated from the whole rock and resuspended in distilled water. After 24 hours of sedimentation, the upper six centimeters of the suspensions, containing approximately the <1.0 μm, were extracted. Then, this fraction was collected on a Millipore filter (0.4 μm) to provide an optimal orientation (Reynolds, 1986), and transferred onto a glass slide. No exchangeable cation was added because Lanson and Besson (1992) compared patterns of Sr-saturated and untreated samples for some typical samples and found no differences. Relative humidity was not controlled during data collection. The oriented specimens were run on a Siemens D500 diffraction system (USGS, Denver, Co) using CuKα radiation, a graphite monochromator, 1° divergence and receiving slits, and the Siemens D5000 software running on a Microvax 2000 (see Table A1 for additional information). Step size and counting times were respectively 0.01–0.02 °2θ and 3–10 seconds.

X-ray pattern numerical treatment—DECOMPXR

The raw patterns were converted to an ASCII format, transferred to an IBM-compatible computer, and treated with DECOMPXR, the decomposition program developed by Lanson (1990, 1992). The structure, performance, and limitations of this program are presented in detail by Lanson (1990), Lanson and Champion (1991), and Lanson and Besson (1992). Basically, the treatment of a raw file begins with a preliminary smoothing to decrease the effect of statistical counting errors. Then, a "background" is subtracted to eliminate most of its contribution to the peaks. Finally, the fit is performed either with a least squares method (Press *et al.*, 1986) or with a non-linear downhill simplex method (Nelder and Mead, 1965; Press *et al.*, 1986) when the least squares method would diverge. Position, FWHM, and intensity of every peak are adjusted until the maximum precision criteria (<0.005 °2θ adjustments on peak position and FWHM, and <0.5 counts adjustment on peak intensity) are achieved. The shape of $K\alpha_1$ and $K\alpha_2$ contributions can be set separately; Lorentzian-, and Gaussian-shaped profiles are available. The calculation algorithms used for X-ray pattern processing (smoothing, background stripping, and elementary peak fitting) are very common and have been detailed by Lanson (1990). Except when specified, all decompositions were performed with Gaussian-shaped peaks for $K\alpha_1$ + $K\alpha_2$ doublets.

Experimental limitations of the decomposition method

The maximum precision criterion used for the fit procedure is smaller than the experimental equipment accuracy and allows one to obtain similar results regardless of the initial values used with the least squares method. To minimize the slight dependence of the results on initial values when using the simplex method (Howard and Preston, 1989), the fit procedure is usually performed twice using the first set of results as the initial values for the second run. Further, the first set of initial values is defined very carefully by analogy with neighboring samples. Because of discrimination

https://doi.org/10.1346/CCMN.1992.0400602 Published online by Cambridge University Press

Table 1. Coherent scattering domain size distributions used to calculate the illite patterns shown in Figure 2. The mean CSDS is the same (12 layers) for all five distributions.

	CSDS value (layers)								
	8	9	10	11	12	13	14	15	16
Distribution 1	0	0	0	0	1	0	0	0	0
Distribution 2	0	0	0	1	1	1	0	0	0
Distribution 3	1	1	1	1	1	1	1	1	1
Distribution 4	2	3	4	5	6	5	4	3	2
Distribution 5	0	1	3	7	5	4	3	2	0

problems between illite and glycolated illitic I/S reflections (for details, refer to Lanson and Champion, 1991), the divergence problems with the least squares method usually occur when treating ethylene-glycol-solvated (EG) patterns. Thus, initial values may be constrained with the results obtained on the AD patterns. The quality of fit is evaluated visually and assumed to be good when the fitted profile, which is the sum of all the elementary peaks, is located within the noise of the experimental data over the complete angular range fitted, and when the general aspect of the experimental pattern (shoulders, inflections, etc.) is respected.

By running a large series of reproducibility tests, Lanson (1990) showed: 1) that the standard deviation on peak characteristics determination is induced mostly by the experimental equipment; 2) that the calculated characteristics are representative of the sample studied; and 3) that this sample is representative of the diagenetic evolution at the stratigraphic level in the studied area. Lanson and Besson (1992) indicate that the error in estimated composition of ordered I/S induced by this standard deviation is less than ±3% illite for ordered I/S. These authors indicate also that a minimum difference of 0.3 and 0.2 °2θ, respectively, on peak position and FWHM is necessary for DECOMPXR to separate the contributions of two phases. However, the difference in one parameter may be much smaller if the other is larger (see Table A2 for examples). By experience (Lanson, 1990; Lanson and Champion, 1991; Lanson and Besson, 1992; Bouchet *et al.*, 1992) the decomposition method presented is well adapted to describe the paragenesis of polyphasic clay mineral assemblages including their evolution with burial and/or time.

Simulation of X-ray diffraction patterns

All the simulations were calculated with the program CALC developed at the University of Orléans. CALC allows calculation of mixed-layer minerals with up to four components and very easy modifications to end-member structures (nature, number, and z-coordinates of the atoms) and junction probabilities. The definition of these junction probabilities is limited to the nearest neighbor interaction (Reichweit = 1). All the simulations are performed assuming illite/smectite hydrated with two water layers, short-range (R = 1) order, and maximum ordering (no SS sequence if % S < 50). As suggested by Lanson and Champion (1991), the structural formulas used for the illite and smectite end-members are, respectively, $K_{0.90}(Si_{3.25}Al_{0.75})(Al_{1.75}Fe_{0.10}Mg_{0.15})O_{10}(OH)_2$ and $M_{0.40}Si_{4.00}(Al_{1.60}Mg_{0.40})O_{10}(OH)_2$, where M is the interlayer cation expressed as an equivalent of a monovalent cation. Their respective d-spacings are set to 10.00 Å and 15.20 Å.

Six coherent scattering domain size (CSDS) distributions ($2 \leq N \leq 5$; $6 \leq N \leq 9$; $11 \leq N \leq 14$; $16 \leq N \leq 19$; $22 \leq N \leq 25$; $36 \leq N \leq 39$) were used to check the influence of this parameter on peak position and FWHM. Very narrow (4 CSDS values) uniform distributions were used, even though real CSDS distributions are likely to be more complicated and to extend over a much larger CSDS range. Five patterns of 100% illite were calculated assuming different CSDS distributions (Table 1) whose mean CSDS values are identical (12 layers). These CSDS distributions (three uniform ones, with one to nine CSDS values, and two triangular ones, one symmetrical and one asymmetrical) were chosen to represent the most frequent simulation hypotheses. On Figure 2, one can note that except for the oscillations related to the interference function maxima, the different patterns, and especially their 8.66 °2θ CuKα (10.20 Å) peaks, are identical. Consequently, the influential parameter is the mean value of the distribution, not its width nor its shape. Obviously, a $11 \leq N \leq 14$ CSDS distribution must not be considered *sensu stricto,* but as the reflection of a distribution having a mean CSDS value of about 12 layers. It is essential to keep this in mind, and not to consider the identified mixed-layer mineral as a unique homogeneous phase, but rather as the reflection of a population of particles that results from a kinetic growth process and whose physicochemical characteristics (i.e, CSDS, illite content of individual particles, and end-member structures, among other parameters) vary about a mean value.

The composition of simulated I/S was varied from 45% to 100% illite (from 45% to 90% illite with 5% illite steps, and from 90% to 100% illite with 2% illite steps). Three different angular ranges were simulated, the first one from 14 to 24 °2θ CuKα (6.3–3.7 Å), the second one from 20 to 35 °2θ CuKα (4.44–2.56 Å), and the last one from 35 to 55 °2θ CuKα (2.56–1.67 Å) to check the 002, 003, and 005 illite peaks and I/S peaks located in the same angular ranges (respectively, 002Ill/003Sm, 003Ill/005Sm, and 005Ill/008Sm).

The FWHM versus peak position plot used for the identification diagram presented in Figure 3 is well adapted to the decomposition method results that provide both position and FWHM for the various elementary peaks fitted to the experimental profile. As a function of these two parameters, the illite content and

https://doi.org/10.1346/CCMN.1992.0400602 Published online by Cambridge University Press

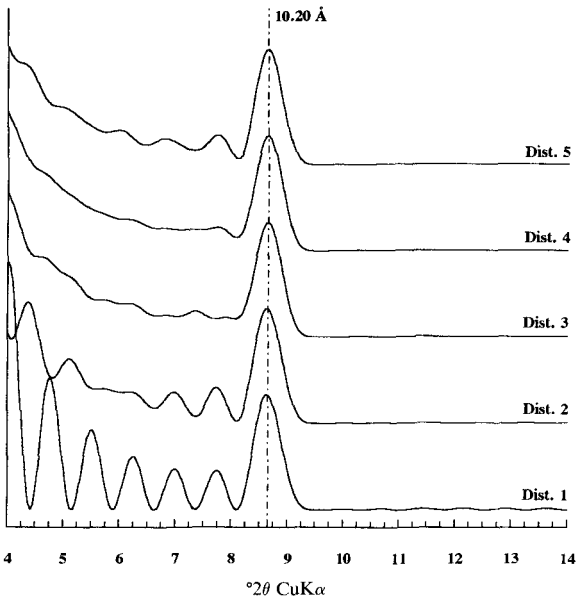


Figure 2. Calculated X-ray diffraction patterns of illite (structural formula: $K_{0.90}$ ($Si_{3.25}Al_{0.75}$) ($Al_{1.75}Fe_{0.10}Mg_{0.15}$) O_{10} $(OH)_2$) assuming five different coherent scattering domain size distributions with the same mean value. The five distributions are described in Table 1.

the mean CSDS of the associated I/S (or any other phase) can be determined. To achieve this, the FWHM versus position plot must be considered as a four axis diagram: the Position- and FWHM-axes are used to plot the characteristics of the elementary peak fitted to the experimental profile, and the other two axes (% illite- and CSDS-) are used to determine the nature of the phase related to this elementary peak. The frame of this identification diagram is neither orthogonal nor linear. It is defined by the plot of simulated diagram characteristics (position and FWHM); their theoretical composition (illite content) and CSDS are used to scale the %illite- and CSDS-axes. To illustrate the use of this type of diagram, three examples are plotted in Figure 3a. Position and FWHM of elementary peak A are respectively, 17.48 and 0.86 °2θ CuKα; thus, Peak A plots very close to the intersection of the 75% illite line with the open diamond (6–9 layers) line. The phase related to peak A is an I/S containing about 75% illite whose mean CSDS is about 7 layers. Peak B, whose position and FWHM are, respectively, 17.63 and 0.47

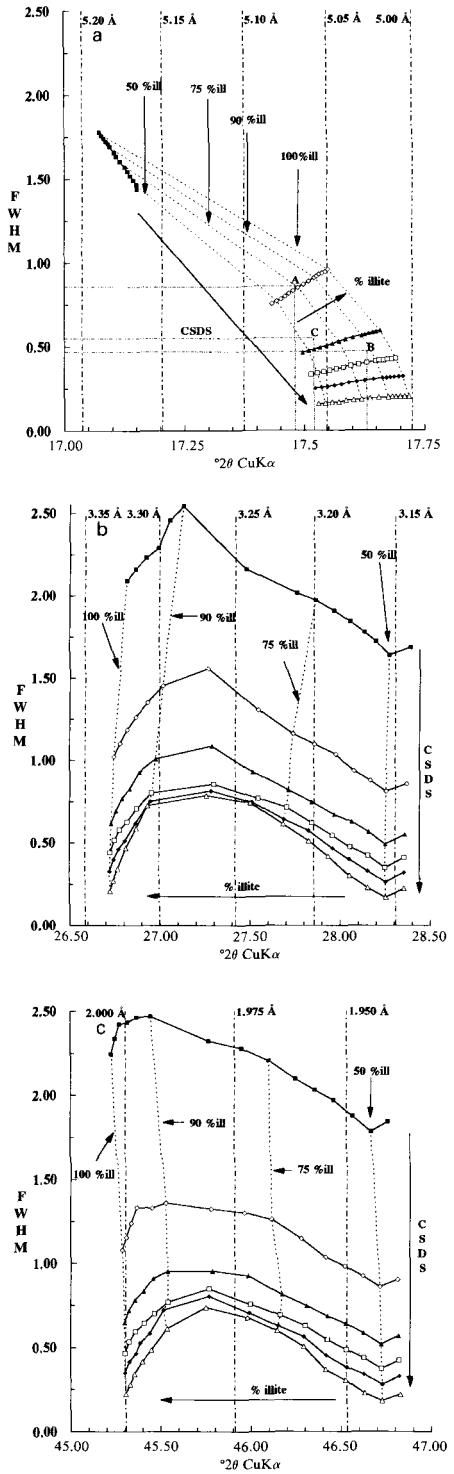


Figure 3. Identification diagrams for ordered (R = 1) mixed-layer illite/smectite; Figure 3a: 002ill/003sm band; Figure 3b: 003ill/005sm band; Figure 3c: 005ill/008 sm band. Position and width (FWHM) are given in °2θ CuKα. Smectite layers are hydrated with two water layers, R1-ordering is maximum. The different patterns represent coherent scattering domain size (CSDS - thickness) distributions (■ $2 \leq N \leq 5$; ◇ $6 \leq N \leq 9$; ▲ $11 \leq N \leq 14$; □ $16 \leq N \leq 19$; ◆ $22 \leq N \leq 25$; △ $36 \leq N \leq 39$). I/S composition varies from 45 to 100% illite (5% illite steps from 45 to 90 % illite, and 2 % illite increments from 90 to 100% illite). Dashed lines represent lines of equal illite content. A, B, and C on Figure 3a are examples used in the text to describe the identification method.

https://doi.org/10.1346/CCMN.1992.0400602 Published online by Cambridge University Press

°2θ CuKα, plots on the 90% illite line and halfway between the solid triangles (11–14 layers) and open squares (16–19 layers) lines. The composition and mean CSDS of the associated phase are, respectively, 90% illite and 15 layers. Peak C (17.52 °2θ CuKα position, and 0.55 °2θ CuKα FHWM) plots between the 50 and 75% illite lines, and between the open diamond (6–9 layers) and the solid triangle (11–14 layers) lines. By interpolating between these values, the I/S contains about 65% illite and its mean CSDS is about 10 layers.

EXPERIMENTAL RESULTS

Illite/smectite mixed-layer identification diagrams

Figure 3 presents the identification diagrams calculated for the three angular ranges defined above. In the 17.7 °2θ CuKα (5.00 Å) region (Figure 3a) one can note that the maximum FWHM is about 1.75 °2θ CuKα, which is the same as that described by Lanson and Besson (1992) for the 5–11 °2θ CuKα (17.6–8.0 Å) region. Peak positions are all lower than 17.72 °2θ CuKα (5.00 Å). Since the interfering reflections are the illite 002 (17.72 °2θ CuKα; 5.00 Å) and the smectite 003 (17.48 °2θ CuKα; 5.07 Å), peak position does not vary much as a function of I/S composition (illite content). Changing the percent illite layers from 50 to 100 in the I/S induces only a 0.11 °2θ CuKα shift in peak position (17.44–17.55 °2θ CuKα; 5.08–5.05 Å), assuming a CSDS distribution from 6 to 9 layers. Changes in the CSDS has a greater influence on peak position than does the number of illite layers. The structure (nature, amount, and z-coordinates of the various atoms constituting the layer) and the basal spacings of both layer types also have significant effects.

In the 26.75 °2θ CuKα (3.33 Å) and the 45.3 °2θ CuKα (2.00 Å) regions (Figures 3b and 3c), the mean CSDS of an I/S phase has a major influence on the FWHM of the XRD peak. The peak position is almost invariant as a function of the mean CSDS for a given illite content. As a consequence, the peak resulting from the overlap of highly illitic phases with varying CSDS, such as those described by Lanson and Champion (1991) in our samples, look very symmetrical (see Figure 6a). Because it is possible to fit such a composite diffraction maximum with only one symmetrical elementary peak (see Figure 6c), it is impossible to get reliable data on CSDS contrasts based only on the decomposition of these higher-angle regions. However, the decomposition of higher-angle peaks (25–50 °2θ CuKα; 3.55–1.8 Å) provides one with very useful additional information to check the consistency of the decomposition performed on the low-angle range (5–11 °2θ CuKα; 17.6–8.0 Å).

The 5–11 °2θ CuKα (17.6–8.0 Å) region, as reported earlier by Lanson and Besson (1992), shows a shift in peak position as well as a difference in FWHM associated with a CSDS variation. The association of both effects induces a major asymmetry that is easy to identify and to model precisely. Consequently, this low-angle range is more appropriate to discriminate such highly illitic phases. However, there are problems; the discrepancy between peak widths measured on experimental and simulated XRD patterns (Reynolds and Hower, 1970; Reynolds, 1989; Lanson and Champion, 1991) makes it impossible to identify accurately the % illite layers in I/S phases in this angular range (5–11 °2θ CuKα; 17.6–8.0 Å). On the other hand, an accurate identification of I/S phases can be performed in the 25–50 °2θ CuKα range (3.55–1.8 Å) since the width of elementary peaks fitted on experimental patterns is similar to the maximum FWHM of simulated patterns, which is about 2.5 °2θ CuKα (Figures 3b and 3c). As a first rough approximation, one can estimate theoretically that 2.0, 1.0, 0.5, and 0.25 °2θ CuKα FWHM correspond, respectively, to CSDS of 3, 5, 12, and more than 20 layers (Figures 3b and 3c). The similarity of the CSDS values obtained for sample C1730 from the various angular ranges (see Figures 5, 7, 8, and 9 and Table 3) also supports this correlation but no direct measurement of the actual particle thickness was performed.

Application to sedimentary series

Experimental peak shape. Lanson and Besson (1992) showed, on both AD and EG patterns, that the diffraction peak of monophasic I/S (WS7–115.45 m) is almost ideally Gaussian in the 5–11 °2θ CuKα (17.6–8.0 Å) range despite theoretical restrictions (Lanson and Besson, 1992) and contrary statements in the literature (Howard and Preston, 1989; Stern *et al.*, 1991). The shape of the diffraction peaks from this sample was also checked at higher angle regions and shown to be symmetrical and basically Gaussian (Figure 4). The fit of peak tails is slightly imperfect, mainly because of background stripping uncertainties. In our experience, it has almost always been possible to fit the I/S peak with a single symmetrical profile whatever the angular range considered (2–50 °2θ CuKα, 44–1.8 Å). However, the micaceous phases and/or chlorite most often overlap the I/S peak, and it is difficult to make a clear statement on experimental peak symmetry.

To check the actual shape of diffraction peaks, experimental profiles of diagenetic samples were fitted with Pearson 7 elementary curves in the 5–11 °2θ CuKα (17.6–8.0 Å) range using Scintag DMS 2000 software (see Appendix). This purely empirical function was used because its exponent may vary to describe all of the usual functions (1.0 for Lorentz shape, 1.5 for modified-Lorentzian, infinite for Gauss). The adjusted value of this exponent will give one a good indication of the actual experimental peak shape for the various elementary peaks. For illite and I/S peaks, this exponent was usually maximized to 10.00 (Table 2), indicating a Gaussian shape, while the adjusted exponent for mica-

https://doi.org/10.1346/CCMN.1992.0400602 Published online by Cambridge University Press

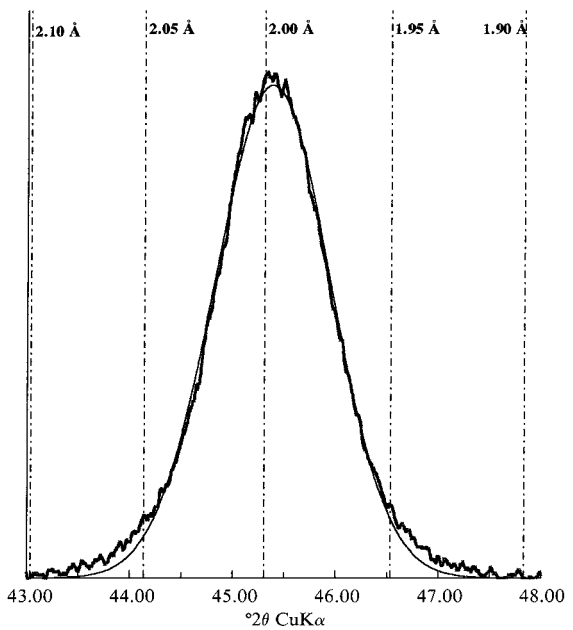


Figure 4. Decomposition of air-dried XRD pattern from sample WS7-115.4 (15% Sm; Inoue *et al.*, 1987). Smooth line represents fit performed with DECOMPXR with one Gaussian-shaped profile.

Table 2. Elementary peak characteristics fitted with DMS2000 software on XRD profiles collected on the Scintag XRD system. Position and FWHM are given in °2θ CuKα. Decompositions are performed assuming either a Gaussian shape or a Pearson7 shape. The maximum exponent value is set to 10.00 on DMS2000 software.

Sample number and peak	Gauss		Pearson7		
	Position	FWHM	Position	FWHM	Exponent
CHV300[1,5]	6.208	0.700	6.230	0.670	1.93
CHV300[2,5]	7.731	1.942	7.642	1.626	10.00
CHV300[3,5]	8.700	0.917	8.643	0.951	10.00
CHV300[4,5]	8.853	0.347	8.859	0.369	2.59
CHV2130[2,5]	8.519	0.896	8.449	0.858	10.00
CHV2130[3,5]	8.778	0.469	8.751	0.438	4.49
CHV2130[4,5]	8.842	0.219	8.855	0.250	1.72
CHV1730[2,6]	17.734	1.548	17.733	1.432	10.00
CHV1730[3,6]	17.857	0.799	17.889	0.619	1.83
CHV1730[4,6]	17.785	0.385	17.754	0.410	0.94
CHV1730[2,7]	26.894	1.613	26.912	1.551	10.00
CHV1730[3,7]	26.744	0.794	26.747	0.863	10.00
CHV1730[4,7]	26.721	0.346	26.723	0.425	2.28
CHV1730[2,8]	45.343	1.799	45.343	1.698	9.99
CHV1730[3,8]	45.324	0.838	45.312	0.794	5.38
CHV1730[4,8]	45.380	0.515	45.387	0.543	8.80

[1] chlorite peak; [2] I/S peak; [3] illite peak; [4] mica-like peak; [5] 001 ill/001 sm band; [6] 002 ill/003 sm; [7] 003 ill/005 sm band; [8] 005 ill/008 sm band.

like and chlorite peaks usually varied from 1.0 to 2.5, indicating a Lorentzian- or modified-Lorentzian function. The origin of these differences in peak shape is unknown, but the peak characteristics obtained assuming either Gaussian or Pearson 7 line profiles are very similar (Table 2). The increased intensity of the chlorite peak "tails" when using a Lorentzian-like peak shape is compensated for by a slightly lower FWHM of the I/S peak and a slight shift of its position. When using DECOMPXR, the shapes of $K\alpha_1$ and $K\alpha_2$ contributions are assumed to be both Gaussian for I/S, illite, and mica-like phases. For the chlorite peak, the shapes of $K\alpha_1$ and $K\alpha_2$ contributions are assumed to be Gaussian and Lorentzian, respectively, to take into account the more Lorentzian character of this peak's shape. These shapes were determined by optimizing the fit (minimum χ^2 value) on numerous experimental XRD patterns.

Mineralogy of the clay fraction and decomposition of the 5–11 °2θ CuKα (17.6–8.0 Å) range. Except for the occasional chlorite peak, all the decompositions performed on the complex diffraction band located between 5 and 11 °2θ CuKα (17.6–8.0 Å, air-dried samples) required three elementary peaks to get a good fit (Lanson and Champion, 1991, Figure 2). As shown by these authors, the three peaks are related respectively to a mica-like phase (sharper peak located between 8.75 and 8.85 °2θ CuKα; 10.10–9.97 Å), an I/S phase (broader peak, lowermost angle region, i.e., from 7.0 to 8.5 °2θ CuKα; 12.6–10.4 Å), and an illite phase (peak with intermediate position and breadth). On Figure 5, the experimental position-FWHM values obtained from experimental patterns are plotted in the identification diagram. The values of the I/S peak (crosses) cannot be checked against theoretical values because of the peak width problem in this angular range (Reynolds and Hower, 1970; Reynolds, 1989; Lanson and Besson, 1992). The FWHM measured on the experimental I/S peak is greater than the width for calculated I/S patterns. The illite peak values (open circles) most often give results consistent with the assumed mineralogy, i.e., illite content between 90% and 100% and mean CSDS from 6 to 12 layers (mostly around 12 layers). The plot of mica-like peak values (solid circles) also is consistent with the assumed mineralogy. The mica-like phase composition varies between 96% and 100% illite and CSDS varies from 20 to 40 layers. This mica-like peak may be related to a detrital muscovite and/or a well-crystallized authigenic illite.

Decomposition of higher-angle peaks. Obviously, the three illitic phases identified on the 5–11 °2θ CuKα (17.6–8.0 Å) range, and by direct observations on TEM (Lanson and Champion, 1991), will give reflections at higher angle. To get consistent results from the various angular ranges, it is necessary to fit these bands with three elementary peaks, as shown on Figure 6a for the 45.3 °2θ CuKα region (2.00 Å). If accessory phases like chlorite, kaolinite, or quartz are detected in the sample, additional elementary peaks are introduced to take into

https://doi.org/10.1346/CCMN.1992.0400602 Published online by Cambridge University Press

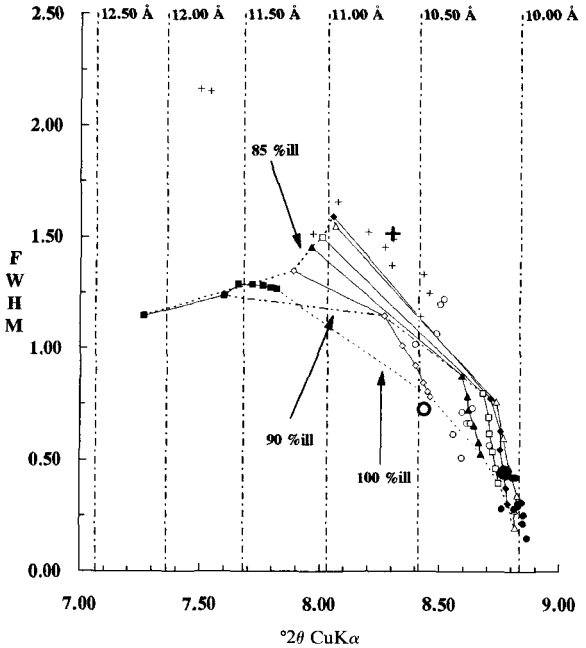


Figure 5. Position and FWHM values of the various elementary peaks from experimental XRD profiles (AD) plotted in the identification diagram for ordered I/S (001ill/001sm band). + I/S phase; ○ illite phase; ● mica-like phase. Enlarged symbols depict positions for sample C1730. Other symbols represent the same CSDS as in Figure 3.

account contributions that may occur in the same angular range.

Theoretically, the FWHM of a diffraction peak is determined mainly by the interference function (Reynolds, 1980), which varies as a function of the CSDS, but not much as a function of the angular range. The values of the FWHM of the interference function calculated for a pure mica phase (d = 9.98 Å, CSDS = 10 layers) and CuKα_1 radiation (λ = 1.540562 Å) are, respectively, 0.80, 0.80, 0.81, 0.83, and 0.86 °2θ CuKα for the 001, 002, 003, 004, and 005 peaks. The respective FWHM of the three elementary peaks fitted to experimental profiles are similar from one angular range to another (Figures 5, 7, 8, and 9). With very few exceptions, the FWHM of the broader peak varies from 1.00 to 2.25 °2θ CuKα, the sharper peak FWHM varies from 0.15 to 0.50 °2θ CuKα, while the peak with intermediate FWHM is 0.50–1.20 °2θ CuKα wide, supporting the validity of the decomposition procedure.

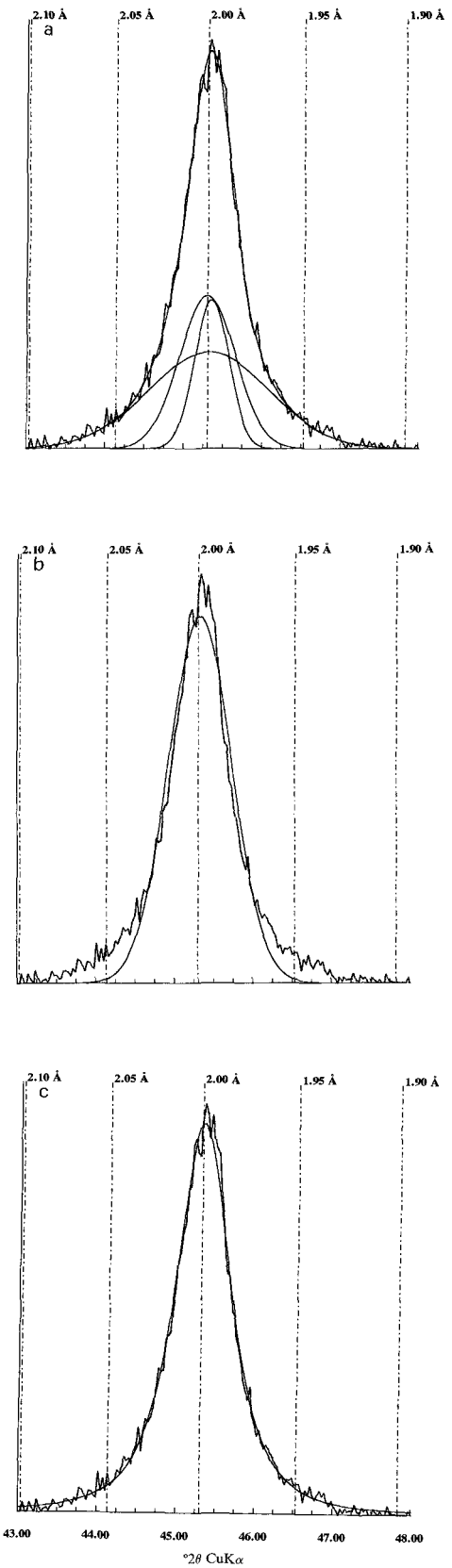


Figure 6: Decomposition of the 45.3 °2θ CuKα (2.00 Å) region of the air-dried XRD pattern of sample C1730. (a) Best fit obtained assuming three Gaussian-shaped elementary curves. (b) Best fit obtained assuming one Gaussian-shaped elementary curve. (c) Best fit obtained assuming one Pearson7-shaped elementary curve.

https://doi.org/10.1346/CCMN.1992.0400602 Published online by Cambridge University Press

One can note (Figure 6) that the diffraction profiles of these polyphasic systems look very symmetrical in the higher-angle regions (25–50 °2θ CuKα; 3.55–1.8 Å) because the CSDS influence on peak position is lower (Reynolds and Hower, 1970; Srodon, 1980). The apparent symmetry of these composite diffraction peaks makes the decomposition procedure more difficult to perform. For example, the illite and mica-like phases present in our samples can only be distinguished by their respective FWHM. But, since their peak positions are identical, it is possible to obtain a good fit with only one elementary peak by modifying the line-profile function. Consequently, it is impossible to get precise information based only on high-angle peak decomposition for systems containing various highly illitic phases. On the other hand, the decomposition of these higher-angle ranges provides additional information to constrain the identification of the phases associated with elementary peaks fitted on the 5–11 °2θ CuKα (17.6–8.0 Å) range (i.e., illitic I/S, illite, and mica-like for our samples).

Uncertainties in background stripping also make it harder to obtain reliable data from the decomposition of these higher-angle regions (25–50 °2θ CuKα; 3.55–1.8 Å). In this range, the background is almost horizontal, but diffracted intensities are low, and it is difficult to define precisely the level of the background. When the background contribution to the diffracted intensity is underestimated, peak "tails" are increased. Consequently, the resulting peak shape tends to be more Lorentzian and FWHM is slightly overestimated.

Decomposition of the 17.7 °2θ CuKα (5.00 Å) region. In order to get consistent information from both the 5–11 °2θ CuKα (17.6–8.0 Å) and the 17.7 °2θ CuKα (5.00 Å) ranges, the decomposition of this latter region must be performed with three elementary peaks. As one can see on Figure 7, the respective FWHM of the observed peaks are similar to those fitted on the 5–11 °2θ CuKα (17.6–8.0 Å) range by Lanson and Champion (1991). This consistency is to be expected theoretically because peak FWHM is constant in both angular ranges for a given phase. As in the 5–11 °2θ CuKα (17.6–8.0 Å) range, experimental I/S peaks are wider than calculated ones, and the identification of I/S with small CSDS is not possible at present in the 17.7 °2θ CuKα (5.00 Å) region.

In addition, it is striking to note the dramatic mismatch between the position of elementary peaks fitted on experimental patterns and the position of diffraction peaks simulated assuming an I/S structure. Since the I/S or illitic nature of these phases has been clearly demonstrated by Lanson and Champion (1991) with XRD decompositions on both AD and EG samples and with chemical analyses, two major hypotheses may be invoked to explain the discrepancy. 1) The very intense (on randomly oriented preparations) 02,11 band

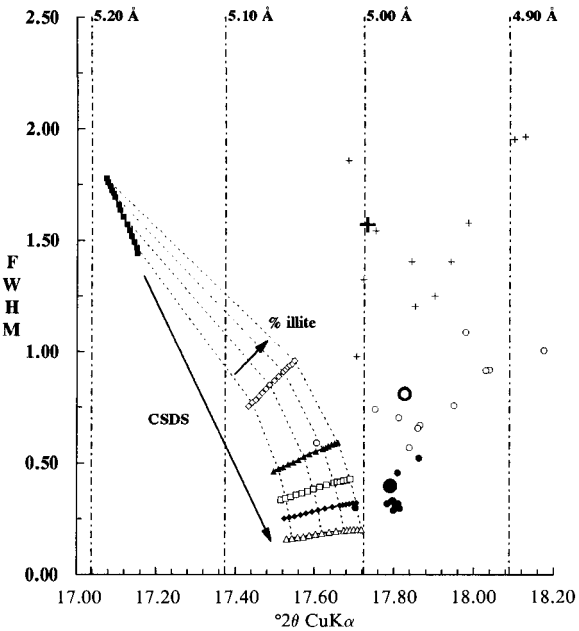


Figure 7. Position and FWHM plots of the various elementary peaks fitted on experimental XRD profiles (AD) plotted in the identification diagram for ordered I/S (002ill/003sm band). Symbols same as Figure 5.

of the mica-like phase could shift the 002 peak toward smaller d-values; however, this influence is probably small because of the preferred orientation of the sample. Furthermore, these two bands are usually well resolved, and it seems unlikely that the 02,11 band could be hidden by the presence of the broad I/S peak. 2) This I/S diffraction peak could result from the interference between the illite 002 band (17.72 °2θ CuKα; 5.00 Å) and the smectite 003 band (17.48 °2θ CuKα; 5.07 Å). Since the two reflections are very close to one another, the peak displacement induced by the interference between smectite and illite layers is very limited, as shown on Figure 3a where peak position varies very little as a function of the illite content for a given CSDS distribution. The basal spacing and the structure of both end-members will have a major influence on the resulting diffraction peak position. The basal spacing for the illite layer assumed for the various sets of simulations is 10.00 Å. However, because of the slightly phengitic nature of the illite end-member (Lanson and Champion, 1991) a 9.95 Å d-value could have been used (Victor Drits, personal communication). This change would give us a better agreement between simulated and experimental peak characteristics, at least for the illite and mica-like phases, with the 002 peak located theoretically at 4.975 Å. Similar problems may be expected for all even 001 reflections of the micaceous phases. In addition, their low intensities also complicate the procedure.

https://doi.org/10.1346/CCMN.1992.0400602 Published online by Cambridge University Press

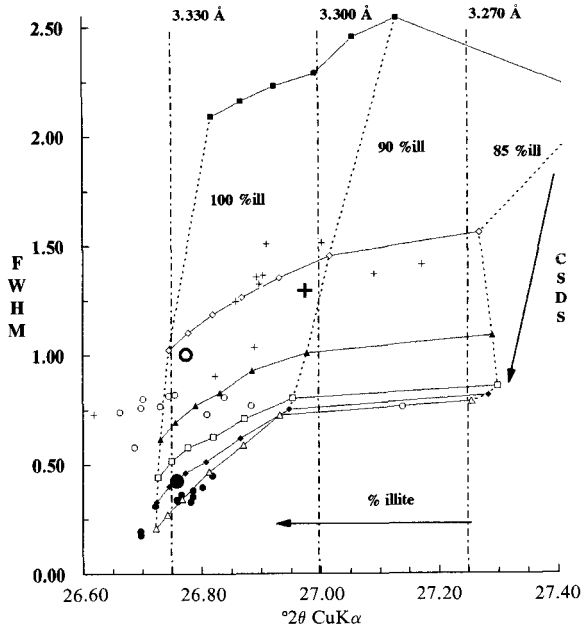


Figure 8. Position and FWHM values of the various elementary peaks fitted on experimental XRD profiles (AD) plotted in the identification diagram for ordered I/S (003ill/005sm band). Symbols same as Figure 5.

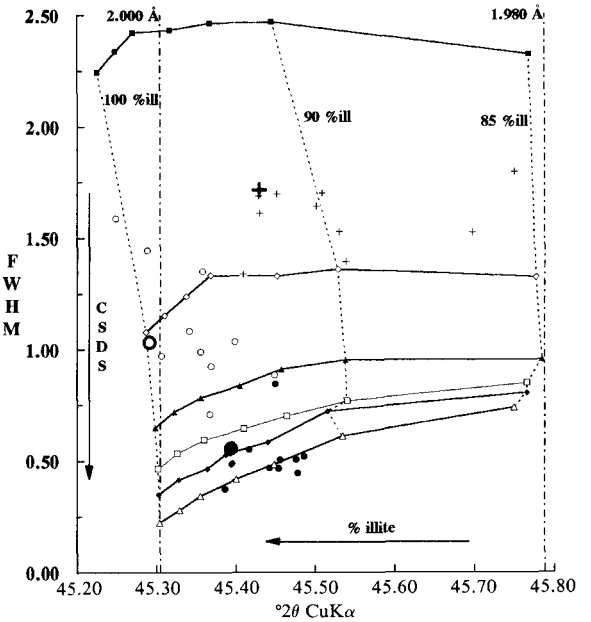


Figure 9. Position and FWHM values of the various elementary peaks fitted on experimental XRD profiles (AD) plotted in the identification diagram for ordered I/S (005ill/008sm band). Symbols same as Figure 5.

Decomposition of the 26.75 °2θ CuKα (3.33 Å) and 45.3 °2θ CuKα (2.00 Å) regions. As for the previous two angular ranges, three elementary peaks were used to fit these domains. On Figures 8 and 9, the respective FWHM of the three elementary peaks are consistent with the decompositions performed in the lower-angle ranges. The FWHM of the mica-like, illite and I/S peaks are, respectively, about 0.30, 0.75 and 1.50 °2θ CuKα. Furthermore, in both angular ranges the peak characteristics decomposed from experimental patterns are very consistent with the ones determined for simulated I/S profiles. This agreement enables one to check precisely the nature of the associated phases given by Lanson and Champion (1991). According to the present simulations, the mica-like phase contains more than 95% illite, with a mean CSDS of about 25–40 layers, which is very consistent with the previous results. The illite phase also has a very high illite content (>95% illite), but the CSDS is much lower (about 6–12 layers) in contrast to the mica-like phase. The composition of the I/S phase is around 90% illite, which is high according to the chemical composition measured on the lath-shaped particles by Lanson and Champion (1991). Their results would indicate an illite content varying from 70% to 85% illite. The CSDS of this I/S phase is about 3–7 layers.

Consistency of the results from the various angular ranges. As described above, the fitted FWHM of the various elementary peaks are unchanged in the different angular ranges. Thus, a good agreement can be expected for the CSDS values determined from the decomposition of different peaks. To check the consistency of the complete identification, one sample (1730 m deep) out of the initial 12 was selected at random to compare the characteristics (% illite and CSDS) of the three phases (mica-like, illite, and I/S) determined in the four angular ranges. The results shown in Table 3 indicate a good agreement. The patterns obtained with the simulation conditions used for this study and the real diffraction patterns are very similar. However, they do not describe the sample perfectly as evidenced by the peak position discrepancy on the 17.7 °2θ CuKα (5.00 Å) band and by the peak width problem for the I/S phase on the 5–11 °2θ CuKα (17.6 Å-8.0 Å) band.

SUMMARY AND CONCLUSIONS

Because the decomposition method is easy and fast to perform, it can be used as a descriptive tool on a great number of samples. Its minor experimental limitations (Lanson, 1990; Lanson and Besson, 1992) make this method a powerful and reliable tool to describe X-ray patterns. However, the warnings formulated by Lanson and Besson (1992) must be obeyed by the user. 1) Verify over the whole angular range (2–50 °2θ CuKα; 44–1.8 Å), and between the various profiles (AD, EG, heated) obtained from the same sample the consistency of the identification (within less than 5% illite for I/S composition and within a few layers for CSDS deter-

https://doi.org/10.1346/CCMN.1992.0400602 Published online by Cambridge University Press

Table 3. Illite content and mean coherent scattering domain size (CSDS) of the phases producing the three elementary peaks fitted to the various diffraction peaks of sample C1730 (data acquisition on the Siemens XRD system). The values are determined by comparison with calculated patterns (see text).

Angular range	Mica-like		Illite		I/S	
	Illite content	CSDS	Illite content	CSDS	Illite content	CSDS
5–11 °2θ CuKα (17.6–8.0 Å)	96%	22–25	100%	6–9	NA	NA
17.7 °2θ CuKα (5.00 Å)	NA	NA	NA	NA	NA	NA
26.75 °2θ CuKα (3.33 Å)	97%	22–25	99%	6–9	91%	6–9
45.3 °2θ CuKα (2.00 Å)	96%	22–25	100%	6–9	92%	4–7

NA: identification data not available because of the mismatch between experimental and simulated position-FWHM values.

mination). 2) Verify that the theoretical pattern, which is the sum of all simulated patterns of phases identified in the sample is similar to the experimental pattern over the whole angular range (2–50 °2θ CuKα; 44–1.8 Å). 3) Check the existence of the phases detected by XRD profile decomposition with direct observations (e.g., TEM associated with chemical analyses, Atomic Force Microscope). These verifications allow one to use the decomposition method not only as a descriptive tool, but also as a reliable and precise identification method for the various argillaceous phases coexisting in the complex clay parageneses that result from the diagenetic alteration of sediments.

In the 25–50 °2θ CuKα (3.55–1.8 Å) range, the agreement between experimental and simulated I/S peak characteristics is good, and it is possible to get an accurate identification of the various phases present in the sample. The mismatches of the I/S peak width observed in the 5–11 °2θ CuKα (17.6–8.0 Å) range (Reynolds and Hower, 1970; Srodon, 1980; Lanson and Champion, 1991) and the gap between experimental and theoretical position-FWHM values in the 17.7 °2θ CuKα (5.00 Å) region are still unresolved. The problems observed in these two angular zones remind us that, despite the good agreement in the 25–50 °2θ CuKα (3.55–1.8 Å) range, the theoretical description of I/S mixed-layer used for the simulation is slightly incorrect. Thus, it will be necessary to consider new simulation hypotheses to refine this description.

Perspectives. Because of important kinetic effects on the smectite-to-illite transformation, the structure of the smectite and illite end-members as well as the composition (illite content) of the I/S particles are very likely to vary about a mean value. The Markovian model for interstratification takes this variability into account as far as the elementary diffracting unit composition goes. Compared to the "identical contents crystal model," the Markovian model induces a slight shift in peak position as well as an interesting peak broadening (Plançon *et al.,* 1983). It should also be useful to simulate the effect of a population of particles whose basal spacings vary about a mean value, since the peak position of the 002 band is probably related to this problem. Kodama *et al.* (1971) showed such a variability of the basal spacing for microcrystalline muscovites induced by the irregular distribution of interlayer cations. More recently, such a variability has been reported by Sato *et al.* (1992) for smectites as a function of the layer charge, the charge location, the expansion energy, the nature of the interlayer cation, and the relative humidity. The effect of the latter parameter has also been shown by Moore and Hower (1986). By modeling low-angle X-ray scattering of smectite gels, Pons *et al.* (1981, 1982) demonstrated the coexistence of various hydration states in the same sample. This may be an additional simulation hypothesis to be tested.

The introduction of faults in the stacking sequence also induces an important peak broadening (Reynolds, 1989). Rather than modeling these defaults by using a different CSDS distribution as Reynolds has done (1985), one might assume the presence of incomplete 2:1 layers (e.g., T-O layers) and/or gibbsite layers in the stacking sequence. The termination of elementary diffracting units on smectitic edges, suggested by Veblen *et al.* (1990) and Güven (1991), also deserves a test to check its influence on XRD profiles. Additionally, models that incorporate the concepts of interparticle diffraction and elementary illite particles (Corbato and Tettenhorst, 1987; Tettenhorst *et al.,* 1990) may be an eventual alternative to the MacEwan crystallite model used in this paper, and others, to simulate X-ray diffraction by mixed-layered clay minerals.

The accuracy and reproducibility of peak characteristic determinations provided by the decomposition method will allow one to check the realism of I/S XRD profile simulation and, consequently, the identification procedure. With the correct simulation of I/S mixed-layer minerals, the decomposition treatment will be useful not only to describe diagenetic trends, but also to identify precisely the various phases present throughout diagenetic series. This is the first step to constrain and to determine the reaction mechanisms of the smectite-to-illite diagenetic transformation and to characterize and to model the kinetics of the various reactions involved in this transformation (Velde and Vasseur, 1992).

https://doi.org/10.1346/CCMN.1992.0400602 Published online by Cambridge University Press

ACKNOWLEDGMENTS

We thank the Institut Français du Pétrole for providing the samples. B.L. acknowledges financial support from Elf Aquitaine Production (Géochimie Minérale Laboratory in Pau, France), and technical support from the U.S. Geological Survey in Denver, USA, where most of this study was done. B.L. thanks D. D. Eberl, G. Besson, and V. Drits for fruitful discussions, and Professors B. Kubler and G. Rumley of the Institut de Géologie in Neuchâtel, Switzerland, for the use of the Scintag diffractometer and helpful discussions.

REFERENCES

Ben Hadj-Amara, A., Besson, G., and Tchoubar, C. (1987) Caractéristiques structurales d'une smectite dioctaédrique en fonction de l'ordre-désordre dans la distribution des charges électriques: I. Etudes des réflexions 001: *Clay Miner.* **22,** 305–318.

Besson, G. (1980) Structures des smectites dioctaédriques. Paramètres conditionnant les fautes d'empilement des ferullets: Ph.D. thesis, Univ. Orléans, France, 153 pp.

Bouchet, A., Lajudie, A., Rassineux, F., Meunier, A., and Atabek, R. (1992) Mineralogy and kinetics of alteration of a mixed-layer kaolinite/smectite in nuclear waste disposal simulation experiment (Stripa site, Sweden): *Appl. Clay Sci.* **7,** 113–123.

Corbato, C. E. and Tettenhorst, R. T. (1987) Analysis of illite-smectite interstratification: *Clay Miner.* **22,** 269–285.

Drits, V. A., Tchoubar, C., Besson, G., Bookin, A. S., Rousseaux, F., Sakharov, B. A., and Tchoubar, D. (1990) *X-ray Diffraction by Disordered Lamellar Structures: Theory and Applications to Microdivided Silicates and Carbons*: Springer-Verlag, Berlin.

Francu, J., Rudinec, R., and Simanek, V. (1989) Hydrocarbon generation zone in the east Slovakian Neogene basin: Model and geochemical evidence: *Geol. Carpath.* **40,** 355–384.

Freed, R. L. and Peacor, D. R. (1989) Variability in temperature of the smectite/illite reaction in Gulf Coast sediments: *Clay Miner.* **24,** 171–180.

Güven, N. (1991) On a definition of illite/smectite mixed-layer: *Clays & Clay Minerals* **39,** 661–662.

Howard, S. A. and Preston, K. D. (1989) Profile fitting of powder diffraction patterns: in *Modern Powder Diffraction, Reviews in Mineralogy* **20,** D.L. Bish and J.E. Post, eds., Miner. Soc. Amer., Washington, D.C. **8,** 217–275.

Inoue, A. (1986) Morphological change in a continuous smectite-to-illite conversion series by scanning and transmission electron microscopies: *J. Coll. Arts & Sci., Chiba Univ.* **B-19,** 23–33.

Inoue, A., Kohyama, N., Kitagawa, R., and Watanabe, T. (1987) Chemical and morphological evidence for the conversion of smectite to illite: *Clays & Clay Minerals* **35,** 111–120.

Inoue, A., Minato, H., and Utada, M. (1978) Mineralogical properties and occurrence of illite/montmorillonite mixed layer minerals formed from Miocene volcanic glass in Waga-Omono district: *Clay Sci.* **5,** 123–136.

Inoue, A., and Utada, M. (1983) Further investigations of a conversion series of dioctahedral mica/smectites in the Shinzan hydrothermal alteration area, northeast Japan: *Clays & Clay Minerals* **31,** 401–412.

Inoue, A., Velde, B., Meunier, A., and Touchard, G. (1988) Mechanism of illite formation during smectite-to-illite conversion in a hydrothermal system: *Amer. Mineral* **73,** 1325–1334.

Inoue, A., Watanabe, T., Kohyama, N., and Brusewitz, A. M. (1990) Characterization of illitization of smectite in bentonite beds at Kinnekulle, Sweden: *Clays & Clay Minerals* **38,** 241–249.

Jennings, S. and Thompson, G. R. (1986) Diagenesis of Plio-Pleistocene sediments of the Colorado river delta, southern California: *J. Sed. Petrol.* **56,** 89–98.

Kodama, H., Gatineau, L., and Méring, J. (1971) An analysis of X-ray diffraction line profiles of microcrystalline muscovites: *Clays & Clay Minerals* **19,** 405–413.

Lahann, R. W. (1980) Smectite diagenesis and sandstone cement: The effect of reaction temperature: *J. Sed. Petrol.* **50,** 755–760.

Lanson, B. (1990) Mise en évidence des mécanismes de transformation des interstratifiés illite/smectite au cours de la diagenèse: Ph.D. thesis, Univ. Paris 6-Jussieu, France.

Lanson, B. (1992) Application de la décomposition des diffractogrammes de rayons-X à l'identification des minéraux argileux: in *Comptes-rendus du colloque rayons-X, Paris 1992,* Siemens, ed., **Vol. 2.**

Lanson, B. and Besson, G. (1992) Characterization of the end of smectite-to-illite transformation: Decomposition of X-ray patterns: *Clays & Clay Minerals* **40,** 40–52.

Lanson, B. and Champion, D. (1991) The I/S-to-illite reaction in the late stage diagenesis: *Amer. J. Sci.* **291,** 473–506.

Moore, D. M. and Hower, J. (1986) Ordered interstratification of dehydrated and hydrated Na-smectite: *Clays & Clay Minerals* **34,** 379–384.

Moore, D. M. and Reynolds Jr., R. C. (1989) *X-ray Diffraction and the Identification and Analysis of Clay Minerals*: Oxford University Press, Oxford.

Nelder, J. A. and Mead, R. (1965) A simplex method for function minimization: *Computer J.* **7,** 757–769.

Plançon, A., Drits, V. A., Sakharov, B. A., Gilan, Z. I., and Ben Brahim, J. (1983) Powder diffraction by layered minerals containing different layers and/or stacking defects. Comparison between Markovian and non-Markovian models: *J. Appl. Cryst.* **16,** 62–69.

Pons, C. H., Rousseaux, F., and Tchoubar, D. (1981) Utilisation du rayonnement synchrotron en diffusion aux petits angles pour l'étude du gonflement des smectites: I. Etude du système eau-montmorillonite-Na en fonction de la température: *Clay Miner.* **16,** 23–42.

Pons, C. H., Rousseaux, F., and Tchoubar, D. (1982) Utilisation du rayonnement synchrotron en diffusion aux petits angles pour l'étude du gonflement des smectites: II. Etude de différents systèmes eau-smectites en fonction de la température: *Clay Miner.* **17,** 327–338.

Press, W. H., Flannery, B. P., Teukolsky, S. A., and Vetterling, W. T. (1986) *Numerical Recepies: The Art of Scientific Computing*: Cambridge University Press, Cambridge.

Reynolds Jr., R. C. (1980) Interstratified clay minerals: in *Crystal Structures of Clay Minerals and Their X-ray Identification,* G. W. Brindley and G. Brown, eds.: Miner. Soc., London **4,** 249–359.

Reynolds Jr., R. C. (1985) NEWMOD: A computer program for the calculation of one-dimensional patterns of mixed-layered clays: R. C. Reynolds, 8 Brook Rd., Hanover, NH 03755, USA.

Reynolds Jr., R. C. (1986) The Lorentz-polarization factor and preferred orientation in oriented clay aggregates: *Clays & Clay Minerals* **34,** 359–367.

Reynolds Jr., R. C. (1989) Diffraction by small and disordered crystals: in *Modern Powder Diffraction, Reviews in Mineralogy* **20,** D. L. Bish and J. E. Post, eds.: Mineral. Soc. Amer., Washington D.C. **6,** 145–181.

Reynolds Jr., R. C. and Hower, J. (1970) The nature of interlayering in mixed-layer illite-montmorillonites: *Clays & Clay Minerals* **18,** 25–36.

Sakharov, B. A. and Drits, V. A. (1973) Mixed-layer kaolinite-montmorillonite: A comparison of observed and

https://doi.org/10.1346/CCMN.1992.0400602 Published online by Cambridge University Press

calculated diffraction patterns: *Clays & Clay Minerals* **21,** 15–17.
Sato, T., Watanabe, T., and Otsuka, R. (1992) Effects of layer charge, charge location, and energy change on expansion properties of dioctahedral smectites: *Clays & Clay Minerals* **40,** 103–113.
Smart, G. and Clayton, T. (1985) The progressive illitization of interstratified illite-smectite from Carboniferous sediments of northern England and its relationship to organic maturity indicators: *Clay Miner.* **20,** 455–466.
Srodon, J. (1979) Correlation between coal and clay diagenesis in the Carboniferous of the upper Silesian coal basin: in *Proc. Int. Clay Conf., Oxford 1978,* M. M. Mortland and V. C. Farmer, eds., Elsevier, Amsterdam, 251–260.
Srodon, J. (1980) Precise identification of illite/smectite interstratifications by X-ray powder diffraction: *Clays & Clay Minerals* **28,** 401–411.
Srodon, J. (1981) X-Ray identification and randomly interstratified illite-smectite in mixtures with discrete illite: *Clay Miner.* **16,** 297–304.
Srodon, J. (1984) X-ray powder diffraction of illitic materials: *Clays & Clay Minerals* **32,** 337–349.
Srodon, J. and Eberl, D. D. (1984) Illite: in *Micas, Reviews in Mineralogy* **13,** S. W. Bailey, ed., Miner. Soc. Amer., Washington D.C. 12, 495–544.
Stern, W. B., Mullis, J., Rahn, M., and Frey, M. (1991) Deconvolution of the first "illite" basal reflection: *Schweiz. Mineral. Petrogr. Mitt.* **71,** 453–462.
Tchoubar, C. (1980) Détermination des paramètres d'ordre et de désordre dans quelques solides à structure lamellaire (silicates, carbones): *Bull. Minéral.* **103,** 404–418.
Tettenhorst, R. T., Corbato, C. E., and Haller, R. I. (1990) The I/S contact in 10 Å-17 Å interstratified clay minerals: *Clay Miner.* **25,** 437–445.
Tomita, K., Takashi, H., and Watanabe, T. (1988) Quantification curves for mica/smectite interstratifications by X-Ray powder diffraction: *Clays & Clay Minerals* **36,** 258–262.
Veblen, D. R., Guthrie, G. D., Livi, K. J. T., and Reynolds, R. C. (1990) High-resolution transmission electron microscopy and electron diffraction of mixed-layer illite/smectite: Experimental results: *Clays & Clay Minerals* **38,** 1–13.
Velde, B. (1985) *Clay Minerals: A Physico-Chemical Explanation of Their Occurrence: Developments in Sedimentology* **40,** Elsevier, Amsterdam, 427 pp.
Velde, B. and Espitalié, J. (1989) Comparison of kerogen maturation and illite/smectite composition in diagenesis: *J. Petrol. Geol.* **12,** 103–110.
Velde, B., Suzuki, T., and Nicot, E. (1986) Pressure-temperature-composition of illite/smectite mixed-layer minerals: Niger delta mudstones and other examples: *Clays & Clay Minerals* **34,** 435–441.
Velde, B. and Vasseur, G. (1992) A kinetic model of the smectite-to-illite transformation based on diagenetic mineral series: *Amer. Mineral.* (in press).
Watanabe, T. (1981) Identification of illite/montmorillonite interstratification by X-ray powder diffraction: *J. Miner. Soc. Jap., Spec. Issue* **15,** 32–41 (in Japanese).
Watanabe, T. (1988) The structural model of illite/smectite interstratified mineral and the diagram for their identification: *Clay Sci.* **7,** 97–114.

(Received 4 August 1992; accepted 10 December 1992; Ms. 2260)

APPENDIX

The present paper demonstrates the use of X-ray pattern decomposition for the identification of complex clay parageneses. Because of the accuracy of peak characteristics (position and FWHM) obtained with this method, it seemed necessary to check if consistent results could be obtained with different diffraction systems and numerical treatment programs. Thus, the same oriented glass slides were run on three different XRD systems whose characteristics are described in Table A1.

As a first step, the raw patterns obtained with the various diffraction systems were converted to an ASCII format, transferred to an IBM-compatible computer, and fitted with DECOMPXR, the decomposition program developed by Lanson (1990, 1992), in order to check that the various diffraction systems could produce comparable results. The differences between these systems are varied: 1) Geometrical and optical differences such as goniometer radius, slit apertures, etc. 2) Operating environment differences, such as the relative humidity, which was not controlled during data collection and differs greatly between Denver (Siemens D500) and Paris (Philips PW 1050/20). In addition to the differences listed in Table A1, the various goniometers were not calibrated with the same standard; however, the consistency of the mica-like peak position and FWHM obtained on the different systems indicated a good agreement. Indeed, the mean variation of the position of this peak (located between 8.75 and 8.85 °2θ CuKα; 10.10–9.97 Å) is 0.038 °2θ CuKα, the mean variation of its FWHM (varying between 0.18 and 0.35 °2θ CuKα) is 0.032 °2θ CuKα. The characteristics (position and FWHM) of the fitted elementary peaks from experimental patterns are given in Table A2, and are very consistent among the different data collection systems. Basically, the variations observed from one diffraction system to another are lower or equal to the standard deviation determined by Lanson (1990) for the estimation of peak characteristics on a single diffractometer. The standard deviations in mean position and FWHM are respectively 0.20 and 0.15 °2θ CuKα for an I/S peak located at 7.25 °2θ CuKα (12.2 Å) and 2.00 °2θ CuKα wide. The standard deviation values decrease as the I/S becomes more illitic and has a larger CSDS.

In the second comparison step, the raw data files were treated (background substraction and decomposition) with the fit programs available on the Philips, Siemens, and Scintag systems to check the consistency between the different pattern treatment programs. Except on the Scintag, where Pearson7 functions were used occasionally to determine the actual shape of the various elementary curves, all the decompositions were performed with Gaussian-shaped peaks. The numerical differences (different background calculation and fit algorithms; convergence criteria) between the various data treatment systems were partly compensated for by the use of the same methodology during the various decompositions. The good agreement of the results obtained on the various systems (Table A3) indicates their mutual consistency. However, one must be very careful using commercially available numerical treatment packages that are not specifically conceived for clay minerals. Automatic peak search criteria, as well as some simplifying and simplified approaches, are not adapted to the very specific characteristics presented by clay mineral XRD profiles such as peak position variability, large FWHM, and severely overlapping peaks (Lanson, 1992).

Intuitively, one can imagine that the background calculation influences the decomposition results. In particular, the intensity level assumed for the background has an effect on the peak "tails," and thus to a certain extent on the shape and the FWHM of decomposed peaks. However, the equation assumed for the background calculation (cubic spline or linear) seems to have little influence on peak characteristics as shown in Table A4.

https://doi.org/10.1346/CCMN.1992.0400602 Published online by Cambridge University Press

Table A1. Experimental settings of the three X-ray diffraction systems used for this study.

Diffractometer	Philips PW1050/20	Siemens D500	Scintag XDS 2000
Location	ENS Paris, France	U.S. Geol. Survey Denver, Colorado	Institut Géologie Neuchâtel, Switzerland
Radiation	Non-monochr. Ni-filtered CuKα	Graphite monochr. CuKα	Non-monochr. CuKα
Divergence slit	1°	1°	2°
Receiving slit	0.1 mm	1°	0.3°
Scatter slit	1°		4° and 0.5°
Tube	fine focus PW2213/20 40 kV, 30 mA	40 kV, 30 mA	SN/60 Rich. Seifert 45 kV, 40 mA
Detector	Proportional Siemens	Scintillation Siemens	Spectral (Peltier-cooled) Kevex PSI 1
Motor and intensity acquisition control	Socabim DACO	Siemens D5000	Scintag DMS 2000
Numerical treatment	DECOMPXR	Siemens D5000	Scintag DMS 2000
Step size	0.01 °2θ	0.01–0.02 °2θ	0.03 °2θ
Counting time	3–12 seconds	3–10 seconds	2 seconds

Table A2. Elementary peak position and FWHM fitted with DECOMPXR (Lanson, 1990) on XRD profiles collected on the Philips, Siemens, and Scintag XRD systems. Position and FWHM are given in °2θ CuKα. Decompositions are performed assuming either a Gaussian shape for both Kα_1 and Kα_2 (I/S, illite, and mica-like peaks) or a Gaussian shape for Kα_1 and a Lorentzian shape for Kα_2 (chlorite peak).

Sample number and peak	Philips ENS–Paris		Siemens USGS–Denver		Scintag Inst. Geol. Neuchâtel	
	Position	FWHM	Position	FWHM	Position	FWHM
CHV300^{1,5}	6.070	0.540	6.208	0.661	6.179	0.652
CHV300^{2,5}	7.299	2.267	7.755	1.986	7.759	1.995
CHV300^{3,5}	8.662	1.123	8.620	0.968	8.668	0.862
CHV300^{4,5}	8.782	0.330	8.811	0.352	8.816	0.337
CHV1000^{1,5}	6.121	0.734	6.230	0.757	6.194	0.798
CHV1000^{2,5}	8.125	1.684	8.126	1.628	8.028	1.715
CHV1000^{3,5}	8.356	0.944	8.391	0.942	8.283	1.019
CHV1000^{4,5}	8.840	0.162	8.842	0.240	8.820	0.294
CHV1475^{1,5}	6.209	0.849	6.657	1.203	6.608	1.307
CHV1475^{2,5}	8.091	1.832	8.192	1.510	8.108	1.455
CHV1475^{3,5}	8.706	0.560	8.708	0.558	8.636	0.570
CHV1475^{4,5}	8.807	0.225	8.846	0.245	8.781	0.244
CHV1550^{1,5}	6.127	1.026	6.363	0.868	6.343	0.734
CHV1550^{2,5}	8.316	1.510	8.254	1.424	8.228	1.414
CHV1550^{3,5}	8.661	0.711	8.591	0.719	8.599	0.773
CHV1550^{4,5}	8.802	0.239	8.798	0.288	8.791	0.273
CHV1850^{1,5}	NA	NA	NA	NA	NA	NA
CHV1850^{2,5}	8.302	1.426	8.444	1.198	8.426	1.183
CHV1850^{3,5}	8.580	0.664	8.677	0.627	8.641	0.622
CHV1850^{4,5}	8.759	0.264	8.840	0.272	8.808	0.287
CHV2130^{2,5}	8.453	1.335	8.424	1.047	8.547	0.950
CHV2130^{3,5}	8.685	0.485	8.636	0.503	8.763	0.402
CHV2130^{4,5}	8.793	0.192	8.756	0.252	8.842	0.180
CHV1850^{1,6}	18.873	0.747	18.807	0.443	18.662	0.548
CHV1850^{2,6}	17.788	1.516	17.877	1.340	17.818	1.575
CHV1850^{3,6}	17.617	0.686	17.829	0.572	17.873	0.625
CHV1850^{4,6}	17.756	0.263	17.798	0.303	17.786	0.264
CHV1850^{1,7}	25.321	0.314	25.297	0.697	25.244	0.504
CHV1850^{2,7}	26.794	1.504	26.815	1.590	26.886	1.828
CHV1850^{3,7}	26.771	0.591	26.780	0.759	26.681	0.717
CHV1850^{4,7}	26.764	0.305	26.768	0.355	26.694	0.332
CHV1850^{2,8}	45.489	2.295	45.503	2.238	45.489	2.436
CHV1850^{3,8}	45.298	1.054	45.407	0.840	45.349	0.852
CHV1850^{4,8}	45.384	0.373	45.434	0.369	45.370	0.343

NA: Data not available. Superscripts same as Table 2 in the text.

https://doi.org/10.1346/CCMN.1992.0400602 Published online by Cambridge University Press

Table A3. Elementary peak characteristics (position and FWHM) fitted with the dedicated data treatment programs (Table 4) on XRD profiles collected on the Philips, Siemens, and Scintag XRD systems. Position and FWHM are given in °2θ CuKα. Decompositions are performed assuming a Gaussian or a Pearson7 (*) shape for both Kα_1 and Kα_2 contributions.

Sample number and peak	Philips ENS–Paris		Siemens USGS–Denver		Scintag Inst. Geol. Neuchâtel	
	Position	FWHM	Position	FWHM	Position	FWHM
CHV300[1,5]	6.070	0.540	6.203	0.496	6.208	0.700
CHV300[2,5]	7.299	2.267	7.538	2.155	7.731	1.942
CHV300[3,5]	8.662	1.123	8.504	1.200	8.700	0.917
CHV300[4,5]	8.782	0.330	8.806	0.423	8.853	0.347
CHV1000[1,5]	6.121	0.734	6.187	0.750	NA	NA
CHV1000[2,5]	8.125	1.684	8.070	1.659	NA	NA
CHV1000[3,5]	8.356	0.944	8.400	1.018	NA	NA
CHV1000[4,5]	8.840	0.162	8.850	0.216	NA	NA
CHV1475[1,5]	6.209	0.849	6.614	1.209	6.458*	0.963*
CHV1475[2,5]	8.091	1.832	8.197	1.523	8.026*	1.432*
CHV1475[3,5]	8.706	0.560	8.707	0.567	8.629*	0.696*
CHV1475[4,5]	8.807	0.225	8.853	0.254	8.817*	0.258*
CHV1850[1,5]	NA	NA	NA	NA	6.360	0.580
CHV1850[2,5]	8.302	1.426	8.431	1.334	8.281	1.478
CHV1850[3,5]	8.580	0.664	8.630	0.666	8.619	0.826
CHV1850[4,5]	8.759	0.264	8.843	0.312	8.830	0.318
CHV2130[2,5]	8.453	1.335	8.422	1.146	8.519	0.896
CHV2130[3,5]	8.685	0.485	8.595	0.511	8.778	0.469
CHV2130[4,5]	8.793	0.192	8.761	0.282	8.842	0.219
CHV1850[1,6]	18.873	0.747	18.821	0.397	18.691	0.491
CHV1850[2,6]	17.788	1.516	17.901	1.252	17.866	1.523
CHV1850[3,6]	17.617	0.686	17.838	0.569	17.888	0.645
CHV1850[4,6]	17.756	0.263	17.814	0.298	17.800	0.264
CHV1850[1,7]	25.321	0.314	NA	NA	25.280	0.560
CHV1850[2,7]	26.794	1.504	26.892	1.359	26.935	1.846
CHV1850[3,7]	26.771	0.591	26.809	0.729	26.723	0.759
CHV1850[4,7]	26.764	0.305	26.786	0.354	26.736	0.337
CHV1850[2,8]	45.489	2.295	45.501	1.646	45.418	2.025
CHV1850[3,8]	45.298	1.054	45.449	0.884	45.384	0.802
CHV1850[4,8]	45.384	0.373	45.478	0.446	45.398	0.347

NA: Data not available. Superscripts same as Table 2 in the text.

Table A4. Elementary peak characteristics (position and FWHM) fitted with DMS2000 on XRD profiles collected on the Scintag XRD system. Position and FWHM are given in °2θ CuKα. Decompositions are performed assuming a Gaussian shape for both Kα_1 and Kα_2 contributions. The background is subtracted assuming either a linear or a cubic spline equation.

Sample and peak	Cubic spline background		Linear background	
	Position	FWHM	Position	FWHM
CHV300[1]	6.198	0.825	6.208	0.700
CHV300[2]	7.718	1.913	7.731	1.942
CHV300[3]	8.715	0.912	8.700	0.917
CHV300[4]	8.853	0.338	8.853	0.347

Superscripts same as Table 2 in the text.

https://doi.org/10.1346/CCMN.1992.0400602 Published online by Cambridge University Press